

Anticancer nanometre-biomissiles carrying a leucine insulator and an antibody complementarity-determining region

Meng Xing¹, Xiaoxia Li², Shanshan An¹, Chongfeng Lan¹, Min Fu¹, Yunfan Shi¹, Yan Huang³, Man Tang¹, Yulin Wan¹, Yuchuan Wang⁴, Jingli Peng¹, Kai Wang¹, Zi-Wei Ye⁵, Shaoping Weng¹, Qiuyun Liu^{1,*}, Jianguo He¹ and Wenliang Zhou¹

¹State Key Laboratory of Biocontrol, Key Laboratory for Improved Variety Reproduction of Aquatic Economic Animals of Guangdong Province, Biomedical Center, School of Life Sciences, Sun Yat-sen University, Guangzhou 510275, China

²School of Materials Science and Engineering, Sun Yat-Sen University, Guangzhou 510275, China

³Division of Life Science, Hong Kong University of Science and Technology, Clear water bay, Kowloon, Hong Kong

⁴Center for Synthetic Biology Engineering Research, Shenzhen Institutes of Advanced Technology, Chinese Academy of Sciences, Shenzhen, Guangdong 518055, China

⁵Department of Microbiology, The University of Hong Kong, Hong Kong

The tumour specificities and potency of miniaturized cancer targeting peptides are among the major issues of current cancer research. Over 100 peptides were evaluated in this study. According to the observations, leucine could sustain the antibacterial and anticancer efficacy of (leucine/lysine)*n* ((L/K)*n*) peptides across different assay conditions, whereas (valine/lysine)*n* ((V/K)*n*) and (isoleucine/lysine)*n* ((I/K)*n*) peptides were less effective. Tumour targeting peptides, consisting of a leucine/lysine peptide and an antibody complementarity-determining region (CDR) fragment against CD47 receptor separated by a leucine₄ insulator, eradicated 100% of the lung cancer A549 cells at 100 μm concentration after 24 h of incubation. It also inhibited tumour growth in a mouse model of colon cancer cells, showing extensive apoptosis at the end of the treatment. Our data suggest that leucine insulators could be effective spacers in the design of targeted or plurispesific peptide drugs given the lack of σ-σ hyperconjugation on β-carbon and the lack of strong van der Waals interactions between the side group and the carbonyl group. Significant reduction of hemolysis by P45-3 with terminal alanine replacement on peptide P129 suggests that biosafety attribute of a peptide can be substantially improved.

Keywords: Anticancer nanometre-biomissiles, antibody complementarity-determining region, consensus peptide sequences, leucine insulator, mouse model.

ANTIMICROBIAL peptides (AMPs) are ubiquitous in the animal and plant kingdoms, and are evolutionarily conserved components of innate immune response^{1,2}. AMPs

can be divided into four major classes based on secondary structures: α-helical, β-sheet, loop and extended peptides. The activities of several AMPs are sensitive to salt concentrations², which reduces their practical applications. The design of artificial AMPs can be an advantage as they may avoid the stresses AMPs generate in the host cells, consequently circumventing the problem of attenuation of AMPs through evolution. Based on the chemical perspective for leucine and β-branched valine and isoleucine (Figure 1)³⁻⁸, a large number of peptides were designed to determine the biological activities for antibacterial and anticancer purposes. Numerous organic acids generated from the Krebs cycle or other pathways possess modest median lethal doses on animals and are negatively charged at physiological pH. Could they also be involved in the cell disruption mechanism for peptides? This study was prompted by the need to understand the mechanism of salt-sensitivity of AMPs and to design active artificial AMPs in the treatment of cancer, bacterial infections, etc. Observations were made on synthetic peptides and their effects on model cell lines and pathological microbes. We found that β-branched valine with 2 γ-methyl groups and to a less extent isoleucine with a single γ-methyl group were among the key factors in the attenuation of AMPs, and non-β-branched leucines could sustain the anticancer and antibacterial activities of (leucine/lysine)*n* ((L/K)*n*) peptides.

Materials and methods

Bacterial strains and reagents

Pseudomonas aeruginosa (1.2464) was purchased from China General Microbiological Culture Collection Center

*For correspondence. (e-mail: lsslqy@mail.sysu.edu.cn)

(CGMCCC), Beijing, China. The multidrug-resistant *Staphylococcus aureus* Y5 strain has been described in a previous study⁹. *Escherichia coli* MG1655 was a kind gift from the *E. coli* Genetic Stock Center (Yale University, New Heaven, CT, USA). *S. aureus* (ATCC6538) was obtained from Guangdong Microbiology Culture Center, Guangzhou, China. Reagents were of analytical grade.

Culture media and equipment

Ten per cent fetal bovine serum (FBS) was obtained from Hyclone (GE Healthcare Life Sciences Inc, Utah, USA), and 1% antibiotics pen-strep was a product of Gibco (Thermo Fisher Scientific Inc, MA, USA). The tumour tissues were observed using a microscope (Olympus BX51WI, Japan). Fluorescence of FITC-labelled peptide in the treatment of bacterial cells was visualized with a confocal laser scanning microscope (Zeiss7 DUO NLO, Zeiss, Jena, Germany). Bacterial cells were examined employing transmission electron microscopy (TEM; JEM 1400 electron microscope, JEOL Ltd, Japan). Scanning electron microscopy (SEM) of cancer cells was also performed (Hitachi S-3400N, Japan).

Peptide synthesis

Solid-phase peptide synthesis was performed by Shanghai BOOTECH Bioscience and Technology Co, Ltd. The peptides were synthesized employing the Fmoc strategy and purified using reversed-phase-high-performance liquid chromatography (RP-HPLC). Characterizations were performed using HPLC and mass spectral analysis. Peptides were at least 98% or 95% pure. Cecropin A was amidated at the carboxyl terminus¹⁰. Magainin 2 was synthesized as an additional control¹¹.

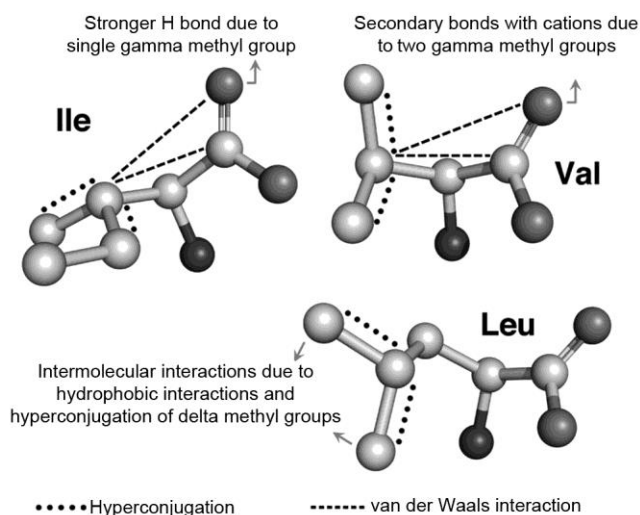


Figure 1. Model depicting chemical perspectives of leucine, isoleucine and valine supported by NMR chemical shift anisotropy and other data.

Cell culture and cell viability assay

Human bronchial epithelial 16HBE14o-cells¹² and lung carcinoma A549 cells¹³ were cultured in DMEM/F12 and DMEM (high glucose) respectively, as recommended by the American Type Culture Collection. Both media were supplemented with 10% FBS. Cell viability was determined using the 3-(4,5-dimethylthiazol-2-yl)-2,5-diphenyl-tetrazolium bromide (MTT; MBCHAM) colorimetric dye method, as previously described¹⁴. In brief, 16HBE14o- and A549 cells were plated overnight in 96-well plates. Then the cells were treated with various peptides and concentrations up to 24 h. The inhibition rate of cell viability was measured using the formula

$$\text{Cell viability inhibition rate (\%)} =$$

$$\frac{\text{Control value A490} - \text{Experimental value A490}}{\text{Control value A490}} \times 100\%.$$

All experimental protocols related to human cells and human tissue in this study were approved by the Committee of the School of Life Sciences at Sun Yat-Sen University, China, and all methods were carried out in accordance with the approved guidelines. Informed consent was obtained from the blood donors (including one of the present author M.T.) for haemolytic assay in accordance with the Declaration of Helsinki. Human lung carcinoma A549 cells were provided by Jun Xu (State Key Laboratory of Respiratory Disease, Guangzhou, China). Human bronchial epithelial 16HBE14o-cells were generously provided by Steven Holgate (University of Southampton, England). The mouse study was performed in strict accordance with the recommendations in the *Guide for the Care and Use of Laboratory Animals* of the National Institutes of Health, USA. The protocol was approved by the Committee on the Ethics of Animal Experiments of Sun Yat-Sen University. Mice were sacrificed by cervical vertebra luxation.

HT29 subcutaneous transplantation tumour animal models

All animal experiments were approved by the Institutional Animal Care and Use Committee of the Sun Yat-sen University. Female Nu/Nu nude mice (Beijing Vital River Laboratories), which were 6–7 weeks and randomized into batches of four in control and five in peptide treatment group, were subcutaneously injected with 1×10^7 HT29 cells on the right abdomen. When the tumour volume had grown up to about 100 mm^3 , $200 \mu\text{l}$ 6 mg/ml peptide P129 was intravenously injected via the tail vein of the treatment mice every other day from day 1 to day 21, while those in the control group underwent the same procedure with phosphate buffer solution (PBS) simultaneously. The weight of the mice and tumour volume were measured with a vernier calliper every two days from

day 1 to day 21, and the tumour volumes were calculated by the following formula

$$V = \pi/6 \times a \times b^2,$$

where a is the length and b is the width of tumor.

After treatment with the peptide, the mice were sacrificed and tumour tissues were subjected to haematoxylin/eosin (H&E) staining assay and TUNEL assay. The H&E staining operations were as follows: the paraffin sections were placed at 60°C atmosphere for 2 h, dewaxed twice in xylene and subsequently were immersed in 100%, 90%, 80% and 70% ethanol respectively. Staining experiments were in strict accordance with the manuals of KeyGEN H&E staining kits. After dehydration in 100% ethanol, the specimens were placed in xylene to obtain transparency; the tumour tissues were observed under a microscope and photographed after being covered with neutral gum.

The TUNEL assay was performed using Merck FragEL™ DNA Fragmentation Detection Kit¹⁵. The procedure was as follows: the dewaxing and hydration operation steps of the paraffin sections were the same as H&E staining. Then 2 mg/ml Proteinase K was diluted to 20 µg/ml in 10 nM Tris pH 8.0. Slides were rinsed with 1 × TBS and the tissue sections were covered with 100 µl of 20 µg/ml proteinase K. Specimens were incubated at room temperature for 20 min. Slides were subsequently rinsed with 1 × TBS. Next 30% H₂O₂ was diluted ten-fold in methanol and the tissue sections were covered with 100 µl of 3% H₂O₂ followed by incubation at room temperature for 5 min. After rinsing the slides with 1 × TBS, the tissue sections were covered with 100 µl of 1 × TdT equilibration buffer followed by incubation at room temperature for 20 min. Next 57 µl TdT labelling reaction mix was mixed gently with 3 µl TdT enzyme on ice for each sample. The 1 × TdT equilibration buffer was carefully blotted from the tissue section and 60 µl of TdT labelling reaction mixture was immediately applied onto each sample and the specimens were covered with a piece of parafilm. Slides were placed in a humidified chamber and incubated at 37°C for 1.5 h. They were rinsed with 1 × TBS and the tissue sections were covered with 100 µl of blocking buffer, followed by incubation at room temperature for 10 min. The blocking buffer was carefully blotted from the tissue sections and 100 µl of diluted 1 × conjugate was immediately applied to the tissue section. Slides were placed in a humidified chamber and incubated at room temperature for 30 min. They were rinsed with 1 × TBS and the entire tissue section was covered with 100 µl of 3,3'-diaminobenzidine (DAB) solution for 10 min. Slides were rinsed with running water. The tissue section was covered with 100 µl of methyl green counterstain solution for 30 sec and the slides were immediately rinsed with running water. The glass slides were dried and mounted on a glass coverslip using neutral gum.

Confocal laser scanning microscopy of bacterial cells

E. coli MG1655 and *S. aureus* (ATCC6538) cultures were propagated to the mid-logarithmic phase respectively. Cells were harvested by centrifugation at 8901 g, washed twice with 10 mM, PBS of pH 7.4 (150 mM NaCl) and resuspended in the same buffer (1.0 × 10⁶ CFU/ml). *E. coli* and *S. aureus* cells were incubated with FITC-labelled peptide P52 (FITC-KKKKLLKKLLK KKKKKKKKLLLLL) at 37°C for 40 min (at final concentrations of 160 and 320 µM respectively). After incubation, a drop of bacterial suspension was coated on a glass slide. Fluorescence was observed using a confocal laser scanning microscope¹⁶. Fluorescent images were obtained with a 489 nm band-pass filter for excitation of FITC.

Transmission electron microscopy of bacterial cells

Samples containing logarithmic *E. coli* MG1655 cells in PBS were incubated with peptides of concentration 160 µM at 37°C, corresponding to at least four of their MIC values for 0.5, 1 and 2 h respectively. Controls containing *E. coli* MG1655 in PBS were incubated without peptides at 37°C. Subsequently, all samples were centrifuged at 7300 g for 1 min. The pellets were fixed using 2.5% glutaraldehyde and stored at 4°C overnight. A drop containing the bacteria was deposited onto a carbon-coated grid and negatively stained with 2% (w/v) purified terephthalic acid (PTA) (pH 7.0). The grids were examined using an electron microscope (JEM 1400)¹⁷.

Scanning electron microscopy of cancer cells

The A549 cells were plated in 24-well, flat-bottom, tissue-culture plates containing sterile circular coverslips and cultured overnight. Then, the cells were treated with indicated peptides and concentrations up to 2 h. They were then washed with PBS twice and fixed with 2.5% glutaraldehyde (v/v) for 1 h at 4°C. Then cells were washed again with PBS followed by dehydration with incremental increases of ethanol (30%, 50%, 70%, 80%, 90% and 100%). After critical-point drying and gold-coating, the samples were observed using SEM¹⁸.

All figures were prepared using ACDSsee 7.0 and Adobe Photoshop 8.0.1.

Results and discussion

Antibacterial and anticancer activities and leucine insulator

Over 100 peptides were synthesized by a commercial vender without a priori consideration of any physico-chemical properties and analysed for their antibacterial and anticancer efficacy. The (leucine/lycine)_n, (L/K)_n

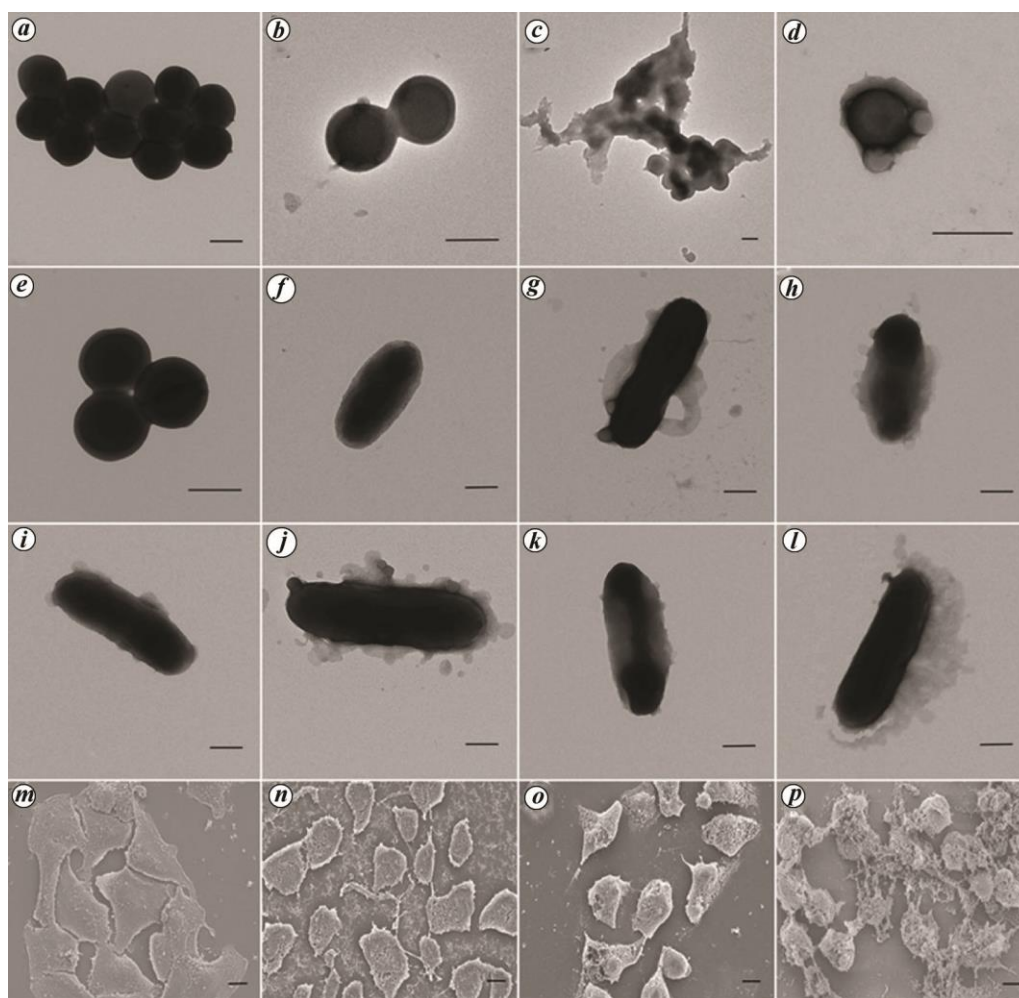


Figure 2. Electron microscopy of bacterial and cancer cells after treatment with peptides. Transmission electron microscopy (TEM) of *S. aureus* (ATCC6538) cells upon incubation with leucine predominant antimicrobial peptide P78 at 160 μ M: (a) control, (b) after 30 min of incubation and (c) after 2 h of incubation. TEM of *S. aureus* (ATCC6538) cells upon incubation with 160 μ M antimicrobial peptide P145: (d) after 30 min of incubation and (e) after 2 h of incubation. TEM of *Escherichia coli* MG1655 cells upon incubation with 160 μ M AMPs: (f) control; (g) after 30 min of incubation with P54; (h) after 2 h incubation with P54; (i) after 30 min of incubation with P83; (j) after 2 h of incubation with P83; (k) after 30 min of incubation with P145 and (l) after 2 h of incubation with P145. Scanning electron microscopy of lung cancer cells A549 upon incubation with 100 μ M peptides: (m) control, (n) peptide P45 at 0.5 h, (o) peptide P45 at 2 h and (p) P129 at 2 h. Scale bar: 500 nm for bacteria and 10,000 nm for cancer cells.

and (phenylalanine/lysine) $_n$, (F/K) $_n$ peptides were potent against bacteria (Supplementary Figure 1). The (F/K) $_n$ peptides were more effective than the (L/K) $_n$, (I/K) $_n$ and (V/K) $_n$ peptides against *E. coli* in LB ($P = 0.000$, Kruskal–Wallis test, two-tailed); (L/K) $_n$ peptides were also more efficacious than (isoleucine/lysine) $_n$, (I/K) $_n$ and (valine/lysine) $_n$, (V/K) $_n$ peptides against *E. coli* ($P = 0.000$, Kruskal–Wallis test, two-tailed); (L/K) $_n$ and (F/K) $_n$ peptides showed no difference against *P. aeruginosa* (0.833, Kruskal–Wallis test, two-tailed), but both were more effective than (I/K) $_n$ and (V/K) $_n$ peptides ($P = 0.000$, Kruskal–Wallis test, two-tailed).

The differences in antibacterial effects of (L/K) $_n$ peptides in the presence and absence of 1% NaCl were statistically significant ($P = 0.000$, Greenhouse–Geisser

correction, general linear model repeated measures). The (L/K) $_n$ peptides were generally slightly stronger in the presence than absence of NaCl. The differences of (F/K) $_n$ peptides in the presence and absence of 1% NaCl were modest but statistically significant ($P = 0.000$, Greenhouse–Geisser correction, general linear model repeated measures). The antibacterial efficacy of the (V/K) $_n$ and (I/K) $_n$ peptides was stronger at 40 μ M when the assays were conducted in NaCl-containing LB medium than in the presence of NaCl versus in the absence of NaCl ($P = 0.000$, $P = 0.000$) respectively, $n = 3$, general linear model repeated measures). However, (V/K) $_n$ peptides, and to a lesser extent (I/K) $_n$ peptides, performed poorly in 1% NaCl-containing LB medium than in NaCl-free LB medium at higher peptide concentrations (data not shown).

a

| | Anticancer peptide | Insulator | Antibody CDR |
|------|-------------------------|------------------|-----------------|
| P45 | LLLLLLKKKLLKKLKKLKKLKKK | | |
| P129 | LLLLLLKKKLLKKLKKLKKLKKK | LLLL | ARGGYTYDDWG |
| P130 | LLLLLLKKKLLKKLKKLKKLKKK | LLLL | YYPYNDGTYNEKFKD |
| P121 | LLLLLLKKKLLKKLKKLKKLKKK | IIIII | ARGGYTYDDWG |
| P55 | LLLLLLKKKLLKKLKKLKKLKKK | | |
| P56 | LLLLLLKKKLLKKLKKLKKLKKK | LLLL | ARGGYTYDDWG |
| P57 | LLLLLLKKKLLKKLKKLKKLKKK | LLLL | YYPYNDGTYNEKFKD |
| P58 | | | ARGGYTYDDWG |
| P59 | | | YYPYNDGTYNEKFKD |
| P75 | LLLLRRRRRRLRRLRRRLRRRR | | |
| P111 | LLLLRRRRRRLRRLRRRLRRRR | LLLLLLLLLLLLLLLL | ARGGYTYDDWG |
| P72 | RRRRLRRLRRLRRLRRLRRLRR | | |
| P128 | RRRRLRRLRRLRRLRRLRRLRR | LLLLLLLLLLLLLLLL | ARGGYTYDDWG |
| P54 | KKKLLKKLKKLKKLKKLKKLKKK | | |
| P63 | LLLLRRLRRLRRLRRLRRLRRL | | |
| P66 | LLLLLLLLRRRRRRLRRLRRRR | | |
| P68 | LLLRRRRRRLRRLRRLRRRRRR | | |
| P71 | RRRRLRRLRRLRRRRRRLLLLL | | |
| P118 | AAAAAKKKLKKLKKLKKLKKK | AAAAA | ARGGYTYDDWG |

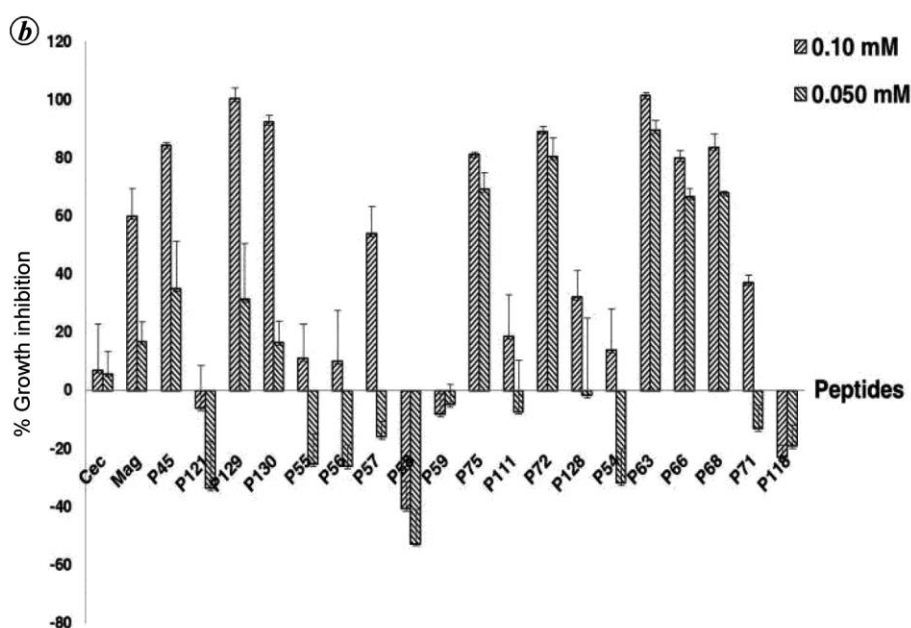


Figure 3. Inhibition rates against lung carcinoma A549 cells using MTT assays. *a*, Tumour targeting peptides consist of an antimicrobial peptide and a CDR fragment of a monoclonal antibody against CD47 receptor separated by a consecutive leucine insulator. P129 carries CDR3, whereas P130 carries CDR1. *b*, Inhibition rates against lung carcinoma A549 cells. Experiments were performed in triplicate with one standard deviation shown. Statistical analysis on treatments at 100 μ M was performed ($n = 3$, growth rate), as follows: P129 ($P = 0.023$ versus control P58); P63 ($P = 0.018$ versus P58; $P = 0.047$ versus P118; two-tailed, Kruskal–Wallis test).

Given the permutations of both L and D isomers in the consensus sequences (L/F/K) $_n$, these AMPs with various lengths have enormous combinatorial diversity. Electron microscopic analysis showed that the leucine-predominant P78 peptide disintegrated the *S. aureus* cells after 2 h of incubation (Figure 2c), while the *E. coli* cells remained largely intact after 30 min treatment with the lysine-predominant peptides P54, P83 and P145 (Figure 2f–i). P145 also did not disrupt the *S. aureus* cells after

treatment (Figure 2d–e), suggesting that an alternative cell damage mechanism may be involved. Conservative replacements of all leucine residues with valine or isoleucine yielded less active peptides (Supplementary Tables 1 and 2, Figure 1). P125 and P127 harbouring only leucine insulator and antibody CDR were ineffective against the bacteria (Supplementary Figure 1).

Tumour targeting peptides, consisting of an antimicrobial peptide described above and a CDR fragment of

an antibody against CD47 receptor^{19,20} separated by a four consecutive leucine insulators, retained activities against bacteria, as shown with peptides P56 and P57 versus their predecessor P55, or with peptides P131 and P132 versus their predecessor P54 (Supplementary Figure 1 and Table 2). In the initial tests for anticancer potential, some of the peptides were more potent than the prototype antibacterial peptides against lung carcinoma A549 cells at modest concentrations (Figure 3), indicating that the designed nanometre-biomissiles (nano-biomissiles) represent an effective strategy targeting at the cell surface markers. CD47 receptors are more abundant in cancer cells than in normal cells, although they are broadly distributed in the body, including erythrocytes¹⁹. One tumour targeting peptide P129 recorded complete (100%) eradication of cancer cells at 100 μ M as determined by MTT assays, versus 84.2% by its predecessor peptide P45 (Figure 3 *b*). The control peptides P58 and P59 recorded growth enhancement activities toward cancer cells, which were antibody CDR alone ($P = 0.023$, P129 versus control P58 at 100 μ M, Kruskal–Wallis test, two-tailed). The anti-*E. coli* activities of tumour targeting peptides P129, P130, P56 and P57 derived from (L/K)*n* peptides at 40 μ M correlated well with anticancer activities at 100 μ M in MTT assays ($P = 0.753$, $n = 3$, covariance analysis). Electron microscopic analysis indicated that P129 resulted in more significant damage on A549 lung cancer cells than P45 (Figure 2 *n–p*). Six consecutive isoleucines in P121 or phenylalanines in P120 were much less effective as insulators in nano-biomissiles when they were tested for antibacterial or anticancer activities (Figure 3; Supplementary Figure 1). (L/F/K)*n* peptides were highly active in antibacterial assays, including observations on a multidrug-resistant *S. aureus* strain Y5 (Supplementary Figure 2).

HT29 subcutaneous transplantation tumour animal models

Low doses of the CD47 targeting peptide P129 exhibited potent anticancer activities in mouse experiments. The HT29 tumour animal model was subjected to tumour growth inhibition test (Figure 4). Mice of the PBS mock control showed poor appetite and adverse physiological responses, while the physiological conditions of the P129 treatment group were significantly better. P129 substantially inhibited tumour growth ($P < 0.05$, general linear model repeated measures; Figure 4 *a*). Mice were sacrificed after the treatment regimen and the tumour sections were subjected to H&E staining (Figure 4 *c* and *d*) and TUNEL assay (Figure 4 *e–f*). The tumour cells of the mock control showed high density with bigger and atypical nuclei, indicating that these cells were in proliferation. The tumour cells of the P129 treatment group exhibited low density with nuclei pyknosis, suggesting

that the peptide could inhibit tumour cell growth and promote cell apoptosis. The TUNEL staining of PBS mock control was virtually DAB-negative, and cells of the P129 treatment group were stained extensively brown, suggesting that tumours of the P129 treatment group experienced wide cell apoptosis. The mock control group recorded one dead mouse on day 23, whereas all mice in the peptide treatment group survived and responded well to the regimen.

Membrane permeability and hemolysis assays

Designed with around 50–70% basic amino acids and the rest hydrophobic amino acids, these peptides usually caused no substantial changes of membrane permeability (Supplementary Figure 3 *a–c*), and some peptides were weakly hemolytic at a concentration of 10 μ M (Supplementary Figure 4). Attenuation of hemolysis by terminal replacements with alanine or valine on the peptides derived from P45 or P149 was observed, whereas minor or modest changes of anti-*E. coli* activities in these peptides were recorded (Supplementary Figure 5). Marked attenuation of hemolysis by P45-3 with terminal alanine substitution on P129 suggests that biosafety profile of a peptide can be improved (Supplementary Figure 4 *c*). Confocal laser-scanning microscopic examination indicated that the FITC-labelled peptide P52 was able to readily penetrate the membranes and accumulate in the cytoplasm of both *E. coli* and *S. aureus* cells (Supplementary Figure 3 *d* and *e*).

The highly enriched particular amino acids in the peptides under study suggest that they are influenced by the chemical properties of the over-represented amino acid residues. The membrane permeability assay of the peptides indicates that they are distinct from the conventional membrane-lytic antimicrobial peptides. Previous studies corroborated the interactions between carbonyl group and γ -methyl groups in valine^{3,4}. Electron delocalization on γ -methyl groups of isoleucine and valine has been suggested by NMR chemical shifts^{21,22}, coupling constants^{3,4,23,24}, and red shifts of the UV and CD spectra relative to those of leucine^{25,26}. The hydrogen bond or other types of secondary weak bonds with carbonyl oxygen could be enhanced by van der Waals forces between the positively charged carbonyl carbon and σ - σ hyperconjugated β -carbon-H. As previously reported, the van der Waals interactions between side chains and the local backbone of proteins determine the intrinsic propensities for β -sheet formation, notably for β -branched amino acids⁵. This may be achieved through enhanced hydrogen bonds.

Other factors that support the above are the large dipole moment²⁷, and longer and shorter bond lengths respectively, in C=O and C β -C γ in valine than leucine, or in C=O and C β -C γ 2 in isoleucine than leucine^{7,8}. Strong

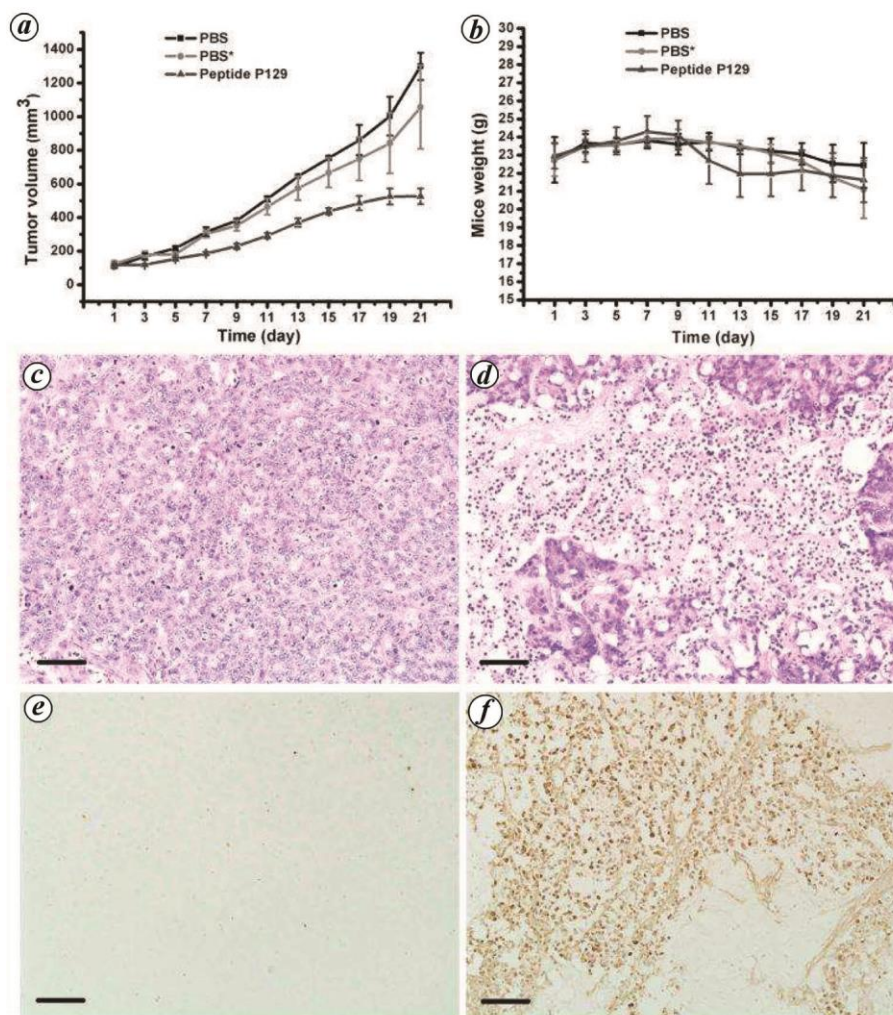


Figure 4. Treatment of tumours with peptide P129 in a HT29 subcutaneous transplantation tumour mouse model. *a*, Tumour growth curves after treatment with PBS (mock control) and P129 with 1.2 mg peptide per injection per two days starting at day 1. Means and standard errors are shown. One mouse bearing a small tumour in the control group died of cancer at day 23. After peptide treatment ($n = 5$ in the peptide treatment group), tumour volumes were reduced significantly ($P = 0.024$ when the dead mouse was included (PBS*, $n = 4$ in the mock control group); $P = 0.000$ when the dead mouse was removed from the mock control data (PBS, $n = 3$)). *b*, Body weight curves after treatment with vehicle PBS and peptide P129. After peptide treatment, body weight changes were not significant ($P = 0.832$ (PBS*), $P = 0.719$ (PBS) versus peptide treatment group). (*c*, *d*) Histological characteristics and (*e*, *f*) TUNEL assays of HT29 tumour tissues (*d*, *f*) after or (*c*, *e*) without treatment with peptide P129. In H&E staining, blue indicates nuclei and red indicates extracellular matrix and cytoplasm. In TUNEL analysis, brown and green stains indicate apoptotic and normal cells respectively. Scale bar: 50 μm .

hydrogen bonding and secondary weak chemical bonding to the carbonyl oxygen of the carboxyl groups were reported to be related to longer than normal C=O bond lengths^{8,28}. There was a marked red shift of the CD spectrum around 200 nm of isoleucine versus leucine at pH 2 relative to pH 7 (ref. 25), which is due to the $n-\pi^*$ transitions of the carboxyl group²⁹. The carbonyl carbon of isoleucine was the most shielded among the amino acids tested as shown by the chemical shift anisotropy of σ_{22} element of the tensor⁸, which supports the presence of stronger hydrogen bonds with the carbonyl oxygen in isoleucine than in leucine (Figure 1). When carbonyl oxygen

of isoleucines in (I/K) peptides forms hydrogen bonds with the protons, it does not weaken the anion trapping and bacteriostatic properties of lysine residues. When carbonyl oxygen of isoleucines forms secondary bonds with K^+ or Na^+ , it attenuates the peptides when isoleucines are situated within lysine clusters. P61 is a hybrid peptide of (I/L/K), and its isoleucine stretch is present only at the peptide terminus; so the effect of isoleucine residues on lysine clusters is less pronounced.

A recent study revealed that leucine replacements at the isoleucine and valine sites have dramatically improved temperature and pH tolerance of a

mini-cellulase³⁰, perhaps explained by weak interactions between carbonyl oxygen of leucine residues and other molecules in the ambient environment. While non- β -branched leucines in most proteins are harmless and help form higher-order structures, they can sustain toxic peptides that disrupt or kill cells. Furthermore, σ - σ hyperconjugation rendered by the δ -methyl groups of leucine may allow inter-molecular van der Waals interactions. This hypothesis is corroborated by NMR chemical shifts^{21,22}, bond lengths (7) and leucine zipper motifs facilitating dimerization³¹.

With two γ -methyl groups valine exhibits longer C=O bond length than that of isoleucine, and its carbonyl oxygen may form stronger secondary bonding with divalent cations than the counterpart of isoleucine. Several peptides show potency in the presence of sodium citrate or/and sodium oxalate (Supplementary Figure 1), suggesting the presence of alternative cell death mechanism using organic acids. Oxalic acid was reported to be an important virulence factor produced by phytopathogenic filamentous fungi³². Given its role in the formation of kidney stones and other diseases, compounds with similar structures to oxalate such as ethanol, acetic acid, pyruvate and alanine have several of beneficial effects in disease treatment and lifespan extension after moderate intake^{33–36}.

As peptides might be degraded over time *in vivo*, no adverse reactions were observed in the peptide treatment group in the HT29 subcutaneous transplantation tumour mouse model. Drug cocktails can be formulated to take advantage of the unique properties of each peptide. Certain bacteria may be inhibited or killed by ion aggregation, and others might be sensitive to locally formed strong acids. Particular cells might be susceptible to insoluble salts like calcium oxalate. Potent (L/K)*n* peptides were generally active regardless of the culture medium. The design of P44, P45, P46, P47, P48, P49, P50, P51, P52 and P55 was to identify the best terminal anchor of the peptides onto the membranes. The anti-*E. coli* and anticancer data indicated that peptides with 5–6 leucines at the terminus were effective.

Conclusion

Tumour targeting peptides consisting of an (L/K)*n* peptide and an antibody CDR fragment separated by a leucine insulator, were effective against cancer cells in *in vitro* assays and an *in vivo* mouse model. The immense combinatorial diversity of (K/L/F)*n* antibacterial peptides warrants further studies.

Conflict of interest: The authors declare that they have no conflict of interest.

- Hoskin, D. W. and Ramamoorthy, A., Studies on anticancer activities of antimicrobial peptides. *Biochim. Biophys. Acta*, 2008, **1778**(2), 357–375.

- Giuliani, A., Pirri, G. and Nicoletto, S. F., Antimicrobial peptides: an overview of a promising class of therapeutics. *Cent. Eur. J. Biol.*, 2007, **2**(1), 1–33.
- Suardiaz, R. *et al.*, Theoretical Karplus relationships for vicinal coupling constants around v1 in valine. *Chem. Phys. Lett.*, 2007, **442**, 119–123.
- Chou, J. J., Case, D. A. and Bax, A., Insights into the mobility of methyl-bearing side chains in proteins from (3)J(CC) and (3)J(CN) couplings. *J. Am. Chem. Soc.*, 2003, **125**(29), 8959–8966.
- Street, A. G. and Mayo, S. L., Intrinsic beta-sheet propensities result from van der Waals interactions between side chains and the local backbone. *Proc. Natl. Acad. Sci. USA*, 1999, **6**(16), 9074–9076.
- Wang, Y. *et al.*, Furthering our understandings on coding SNPs: β -branched amino acids in diseases. *Science*, 2017; <http://science.sciencemag.org/content/350/6265/1262/tab-e-letters>.
- Gould, R. O., Gray, A. M., Taylor, P. and Walkinshaw, M. D., Crystal environments and geometries of leucine, isoleucine, valine and phenylalanine provide estimates of minimum nonbonded contact and preferred van der Waals interaction distances. *J. Am. Chem. Soc.*, 1985, **107**(21), 5921–5927.
- Gu, Z., Zambrano, R. and McDermott, A., Hydrogen bonding of carboxyl groups in solid-state amino acids and peptides: comparison of carbon chemical shielding, infrared frequencies, and structures. *J. Am. Chem. Soc.*, 2002, **116**(14), 6368–6372.
- He, R. *et al.*, A combinatorial yeast overlay method for the isolation of antibacterial oligopeptides. *Proc. Natl. Acad. Sci. India Sect. B*, 2014, **84**(4), 1069–1075.
- Steiner, H., Sequence and specificity of two antibacterial proteins involved in insect immunity. *Nature*, 1981, **292**, 246–248.
- Zasloff, M., Magainins, a class of antimicrobial peptides from *Xenopus* skin: isolation, characterization of two active forms, and partial cDNA sequence of a precursor. *Proc. Natl. Acad. Sci. USA*, 1987, **84**(15), 5449–5453.
- Cozens, A. L. *et al.*, Cfr expression and chloride secretion in polarized immortal human bronchial epithelial cells. *Am. J. Respir. Cell Mol. Biol.*, 1994, **10**(1), 38–47.
- Lieber, M. *et al.*, A continuous tumor-cell line from a human lung carcinoma with properties of type II alveolar epithelial cells. *Int. J. Cancer*, 1967, **17**(1), 62–70.
- Warshamana-Greene, G. S. *et al.*, The insulin-like growth factor-I receptor kinase inhibitor, NVP-ADW742, sensitizes small cell lung cancer cell lines to the effects of chemotherapy. *Clin. Cancer Res.*, 2005, **11**(4), 1563–1571.
- Chen, W. *et al.*, Co-delivery of doxorubicin and siRNA with reduction and pH dually sensitive nanocarrier for synergistic cancer therapy. *Small*, 2014, **10**(13), 2678–2687.
- Park, K. H. *et al.*, Cell specificity, anti-inflammatory activity, and plausible bactericidal mechanism of designed Trp-rich model antimicrobial peptides. *Biochim. Biophys. Acta*, 2009, **1788**(5), 1193–1203.
- Joshi, S. *et al.*, Interaction studies of novel cell selective antimicrobial peptides with model membranes and *E. coli* ATCC 11775. *Biochim. Biophys. Acta*, 2010, **1798**(10), 1864–1875.
- Hilchie, A. L. *et al.*, Pleurocidin-family cationic antimicrobial peptides are cytolytic for breast carcinoma cells and prevent growth of tumor xenografts. *Breast Cancer Res.*, 2011, **13**(5), R102.
- Willingham, S. B. *et al.*, The CD47-signal regulatory protein alpha (SIRPa) interaction is a therapeutic target for human solid tumors. *Proc. Natl. Acad. Sci. USA*, 2012, **109**(17), 6662–6667.
- Yasufumi, K. *et al.*, Humanized anti-CD47 antibody. 2006, Patent No. EP1693385.
- Zhang, H., Neal, S. and Wishart, D. S., RefDB: a database of uniformly referenced protein chemical shifts. *J. Biomol. NMR*, 2003, **25**, 173–195.

22. Wishart, D. S. *et al.*, ^1H , ^{13}C and ^{15}N random coil NMR chemical shifts of the common amino acids. I. Investigations of nearest-neighbor effects. *J. Biomol. NMR*, 1995, **5**(1), 67–81.
23. Penkett, C. J. *et al.*, NMR analysis of main-chain conformational preferences in an unfolded fibronectin-binding protein. *J. Mol. Biol.*, 1997, **274**(2), 152–159.
24. Smith, L. J. *et al.*, Analysis of main chain torsion angles in proteins: prediction of NMR coupling constants for native and random coil conformations. *J. Mol. Biol.*, 1996, **255**(3), 494–506.
25. Nishino, H. *et al.*, The pH dependence of the anisotropy factors of essential amino acids. *J. Chem. Soc. Perkin Trans. 2*, 2002, **23**(3), 582–590.
26. Matsuo, K. *et al.*, Vacuum-ultraviolet circular dichroism of amino acids as revealed by synchrotron radiation spectrophotometer. *Chem. Lett.*, 2002, **5**(8), 826–827.
27. Ganesan, A., Brunger, M. J. and Wang, F., A study of aliphatic amino acids using simulated vibrational circular dichroism and Raman optical activity spectra. *Eur. Phys. J. D*, 2013, **67**(11), 229.
28. Ichikawa, M., The effect of hydrogen bonding on the bond lengths and angles in the carboxyl group. *J. Chem. Crystallogr.*, 1979, **9**(2), 87–105.
29. Snyder, P. A., Vipond, P. M. and Johnson, W. C., Circular dichroism of the alkyl amino acids in the vacuum ultraviolet. *Biopolymers*, 1973, **12**(5), 975–992.
30. Xiao, Y. *et al.*, *Neurospora crassa* tox-1 gene encodes a pH- and temperature-tolerant mini-cellulase. *J. Agric. Food Chem.*, 2016, **64**(23), 4751–4757.
31. E, Z. G., Zhang, Y. P., Zhou, J. H. and Wang, L., Mini review roles of the bZIP gene family in rice. *Genet. Mol. Res.*, 2014, **13**(2), 3025–3036.
32. Godoy, G., Steadman, J. R., Dickman, M. B. and Dam, R., Use of mutants to demonstrate the role of oxalic acid in pathogenicity of *Sclerotinia sclerotiorum* on *Phaseolus vulgaris*. *Physiol. Mol. Plant Pathol.*, 1990, **37**(3), 179–191.
33. Chow, F. C., Dysart, M. I., Hamar, D. W. and Udall, R. H., Control of oxalate urolithiasis by DL-alanine. *Invest. Urol.*, 1975, **13**(2), 113–116.
34. Chuang, M. H. *et al.*, The lifespan-promoting effect of acetic acid and Reishi polysaccharide. *Bioorg. Med. Chem.*, 2009, **17**(22), 7831–7840.
35. Paganini-Hill, A., Kawas, C. H. and Corrada, M. M., Type of alcohol consumed, changes in intake over time and mortality: the Leisure World Cohort Study. *Age Ageing*, 2007, **36**(2), 203–209.
36. An, S. *et al.*, Functional duality of ethanol on cancer. *Med. Hypotheses*, 2019, **122**, 124–125.

ACKNOWLEDGEMENTS. This work was supported by grants from the Science and Technology Transformation Programme of Sun Yat-sen University of China (No. 33000-18843234) and Guangzhou Science and Technology Programme (No. 201804010328) to Q. L.; China Agriculture Research System (47), The National Key Technology R&D Programme (2012BAD17B03), and The National Key Technology R&D Programme (2011BAD13B10) to J. H. and The National Natural Science Foundation of China (21601209) to Y. W. We thank D. Augustyniak for the ML-35 strain and Guangchuang Yu for help with statistical analysis. We also thank Bo Yu, Li Xu, Jing Li, Fan Yang and Xiang Zhu for suggestions and technical assistance and Ms. Yan Shi at Sun Yat-sen University for editorial assistance. Qiuyun Liu, Jianguo He and Wenliang Zhou co-supervised the work. Meng Xing, Xiaoxia Li and Shanshan An contributed equally to this project.

Received 21 March 2019; revised accepted 7 October 2020

doi: 10.18520/cs/v120/i1/177-185